metals

MDPI

Article

Effects of Partially Replacing Mo with Nb on the Microstructure and Properties of High-Strength Low-Alloy Steel during Reverse Austenization

Liang Luo [1], Jiajun Zhang [1], Hao Fu [1,2], Fuhu Chen [1,*], Jianchun Qin [1,*] and Yimin Li [1,3]

[1] School of Electronic Engineering, Guangxi University of Science and Technology, Liuzhou 545006, China
[2] Engineering Training Center, Jiujiang Vocational and Technical College, Jiujiang 332007, China
[3] State Key Laboratory of Powder Metallurgy, Central South University, Changsha 410083, China
* Correspondence: chenfuhu@gxust.edu.cn (F.C.); qinjianchun988@gxust.edu.cn (J.Q.)

Abstract: This study investigated the effects of partially replacing expensive Mo with cheaper Nb on the microstructure and properties of high-strength low-alloy (HSLA) steel during reverse austenisation. The mechanical properties of the steel in the hot-rolled state were lower with a partial replacement of Mo by Nb. However, after pre-tempering and reheating and quenching, the strength increased greatly while the ductility and toughness did not decrease much. Thus, the negative effects of replacing Mo with Nb were mostly alleviated, and a good balance between strength, ductility and toughness was achieved. After heat treatment, the mass percentage of precipitates increased substantially, which helped to pin grain boundaries during austenisation. The percent of high-angle grain boundaries greatly increased while the average effective grain size decreased, which improved grain refinement. The results showed that combining a partial replacement of Mo by Nb with heat treatment allows the microstructure and mechanical properties of HSLA steel to be effectively controlled while improving the balance between cost and performance. These findings provide valuable insights into the preparation and design of steels with similar microstructures.

Keywords: HSLA steel; mechanical properties; austenising; Mo; Nb

Citation: Luo, L.; Zhang, J.; Fu, H.; Chen, F.; Qin, J.; Li, Y. Effects of Partially Replacing Mo with Nb on the Microstructure and Properties of High-Strength Low-Alloy Steel during Reverse Austenization. *Metals* **2024**, *14*, 896. https://doi.org/10.3390/met14080896

Academic Editor: Andrea Di Schino

Received: 20 June 2024
Revised: 23 July 2024
Accepted: 29 July 2024
Published: 6 August 2024

1. Introduction

Research on enhancing the strength of steel without compromising ductility and toughness has mostly focused on optimising the microstructure and chemical composition to better balance the mechanical properties [1–6]. Innovative alloy designs and heat treatment processes have been proposed to control and refine the microstructure, and they have proven effective strategies for enhancing the strength while maintaining or improving its plasticity and toughness [7–9]. High-strength low-alloy (HSLA) steels are designed by microalloying elements such as titanium (Ti), niobium (Nb), vanadium (V) and molybdenum (Mo) to improve the mechanical properties [10–13]. These elements easily combine with atoms in steel to form nanoscale (<100 nm) carbides, nitrides and carbonitrides with higher strength than the steel matrix. When the precipitate phase is distributed at grain boundaries, it can pin the grain boundaries and hinder grain growth [14–16]. Ti, V and Nb all have high melting points, and they are often added in combination to obtain small carbonitrides with large volume fractions to improve the strength of HSLA steel. Mo plays a unique role in HSLA steel because its differences and interactions with iron (Fe), carbon (C) and other alloying elements in terms of the atomic structure, size and crystal lattice can improve both strength and toughness. Many studies have found that Mo does not precipitate separately in austenite but in a composite form when added in combination with Nb, Ti and V [17–20]. The addition of Mo further refines second-phase particles in the steel [21] and greatly improves the precipitation-strengthening effect. Mo can also reduce the coarsening rate of second-phase particles to improve the high-temperature performance

of the steel. However, Mo is relatively expensive compared to the other microalloying elements, and a large amount of Mo needs to be added to improve the results.

One approach to improving the microstructure and properties of HSLA steel is by heat treatment [22–27]. Heat treatment is often used in conjunction with microalloying to achieve better results. For HSLA steels, it is difficult for fine precipitates such as carbonitrides to precipitate fully and uniformly during the rolling process, which impedes the effectiveness of precipitation strengthening. Therefore, improving the strength and plasticity of HSLA steel can not only be achieved by optimising the rolling process. The modification of heat treatment processes is an essential method to obtain superior microstructure and mechanical properties. A proper heat treatment process combined with microalloying elements is used to achieve the purpose of grain refinement. However, the role that microalloying elements play in heat treatment processes is still unclear and requires further exploration.

In this study, hot-rolled steel was first pre-tempered to precipitate more second-phase particles in the matrix. Subsequently, a heat treatment process comprising reheating and quenching was carried out to use the second-phase particles to pin grain boundaries during the reverse austenisation process, which helped to refine grains and substructures to obtain HSLA steel with excellent strength and matching plasticity and toughness. The objective of the study was to evaluate the roles that the microalloying elements Mo and Nb play in the heat treatment process and the effects of partially replacing expensive Mo with cheaper Nb. This work was expected to offer new insights into the preparation of HSLA steels and other steels with similar microstructures and improve the balance between cost and performance.

2. Materials and Methods

Table 1 presents the chemical compositions of the two HSLA steels considered in this study: GQ0 and GQ1. GQ1 was derived from GQ0 by a partial substitution of Nb with Mo. Two HSLA steels have a high Ti content, the purpose of which is to improve the precipitation-strengthening effect of steel. Both steels were melted in a vacuum induction furnace and cast into 25 kg ingots, which were then forged into 100 mm thick slabs. For the hot-rolling process, the slabs were homogenised at 1250 °C for 2 h, which was followed by controlled rolling and cooling. The HSLA steels were rolled for 8 passes. The cumulative reductions of the first three passes were 0.6 (rough rolling), the cumulative reductions of the fourth to eighth passes were 0.8 (finish rolling), and the reductions of each pass were between 0.25 and 0.3. The finishing rolling temperature was set at 870 °C, and the slabs were laminar-cooled at a rate of 15 °C/s to 615 °C before being air-cooled to room temperature. The final thickness of the steel plate was 8 mm. For the heat treatment process, the slabs were pre-tempered at 550 °C for 3 h, reheated to 880 °C for 5 min and then quenched in water. Figure 1 illustrates the hot-rolling and heat treatment processes. The original hot-rolled steels retained the designations of GQ0 and GQ1, and heat-treated steels were designated as GQ0-HT and GQ1-HT, respectively.

Table 1. Chemical composition of the experimental steels.

Type	C	Si	Mn	Ti	Cr	Mo	Nb	Fe
GQ0	0.25–0.28	0.25–0.30	1.0–1.3	0.1–0.2	0.3–0.4	0.25–0.30	--	Bal.
GQ1						0.10–0.15	0.05–0.09	

The microstructure was examined with scanning electron microscopy (SEM; FEI Inspect F50, ZIESS, Oberkochen, Germany). Samples with dimensions of 10 mm × 8 mm × 5 mm were extracted from the slabs by electrical discharge machining. The samples were then ground, polished and etched with 4% nitric acid in alcohol. The samples were rinsed with water and anhydrous ethanol and dried. The high-angle grain boundary and effective grain size (EGS) were analysed by electron backscatter diffraction (EBSD) using the SEM system (FEI Inspect F50) at a step length of 0.5 μm. The data were interpreted by using the Oxford Instruments Channel 5HKL 2.0 programme package. The phase and carbide

morphologies were observed at high resolution by transmission electron microscopy (TEM; FEI Talos F200X, Hillsboro, OR, USA). Samples for TEM analysis were prepared from a 3 mm diameter disc thinned by using a Gatan 691 ion-milling machine. The precipitates were calculated and quantified by the phase analysis method. Precipitates were extracted by electrolysis under the conditions of a 3% HCI + 5% glycerol + 2.5% (g/L) citric acid methanol solution, current density I = 0.05–0.08 A/cm^2 and temperature T = −5 to 10 °C. The size distribution of precipitates was tested by small angle X-ray scattering (SAXS; SmartLab, Tokyo, Japan) using a Co target with an incident slit of 40 μm, scattering slit of 0.1 mm and receiving slit of 0.02 mm. Tensile tests were performed at room temperature by using an electronic universal testing machine (WDW-300-I, Zhongyi, Jinan, China). Low-temperature Charpy V-notch impact tests were conducted at −20 °C by using a microcomputer-controlled low-temperature automatic impact tester (JBD-300J-60, Keshen, Jinan, China). The results were recorded as the averages from three measurements for the tensile tests and five measurements for the impact tests.

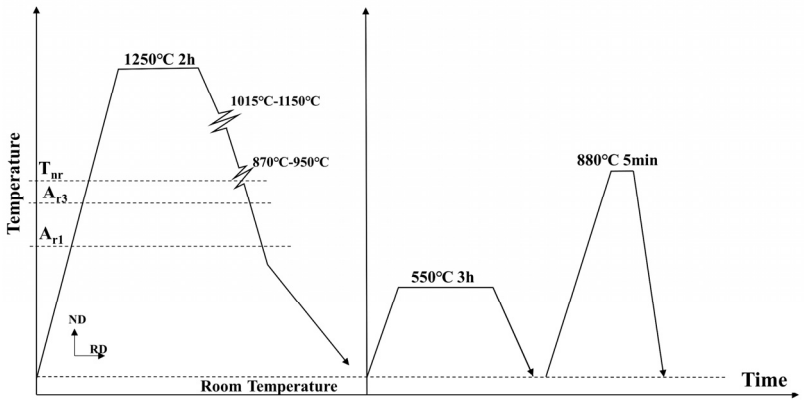

Figure 1. Hot-rolling and heat treatment processes for the steels.

3. Results and Discussion

3.1. Effect of Partial Replacement of Mo by Nb on the Mechanical Properties

Figure 2 shows the mechanical properties of the steel samples. GQ1 had a lower strength, elongation and −20 °C impact absorption energy than GQ0. In particular, the impact absorption energy was only 27% that of GQ0. Thus, in the case of the current replacement ratio, partially replacing Mo with Nb initially resulted in comprehensively lower mechanical properties of the steel after hot-rolling treatment. After heat treatment, however, both GQ0-HT and GQ1-HT showed substantial increases in strength to almost the same value, while the elongation and impact absorption energy did not decrease substantially. Thus, the reduction in plasticity and toughness was controlled. GQ1-HT showed a 144.7% increase in impact absorption energy compared to GQ1. In addition, the impact absorption energy of GQ1-HT was 79.5% that of GQ0-HT, which greatly narrowed the gap compared with between GQ1 and GQ0. Thus, heat treatment greatly alleviated the negative effects of replacing Mo with Nb. These findings indicate that the heat treatment process of pre-tempering, reheating and quenching effectively optimised the balance between ductility and toughness while maintaining a high strength. This heat treatment enhanced the overall material properties, which indicates that it is a promising approach for the development of high-performance HSLA steels.

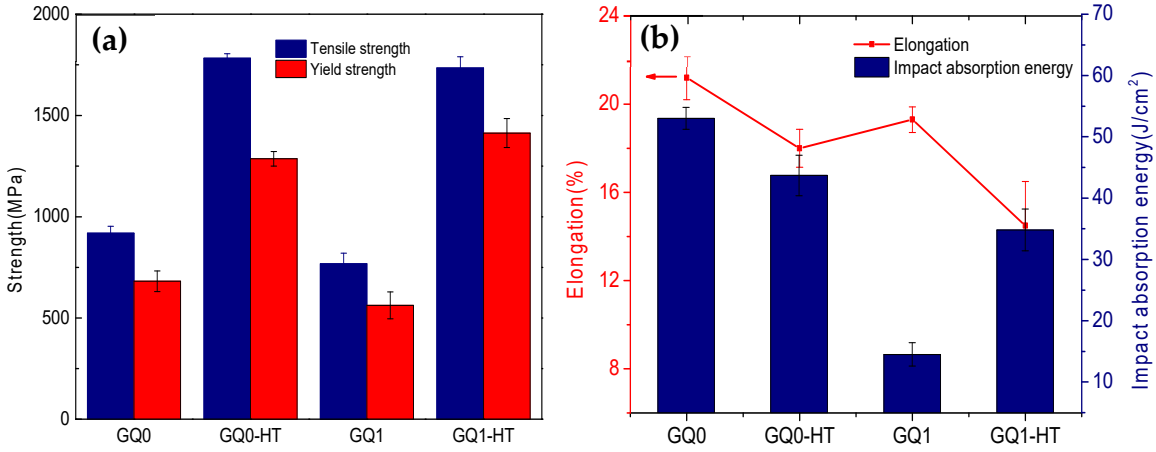

Figure 2. Mechanical properties of hot-rolled and heat-treated steel samples: (**a**) tensile strength and yield strength; (**b**) elongation and impact absorption energy.

3.2. Effect of Partial Replacement of Mo by Nb on the Microstructure

Figure 3a,b show the microstructural morphology of the two experimental steels after the hot-rolling treatment. Both GQ0 and GQ1 comprised granular bainite, ferrite and small amounts of martensite/austenite islands. The main difference was that GQ1 had a slightly coarser microstructure than GQ0. Figure 3c and d show the microstructural morphology of the steels after heat treatment. Both GQ0-HT and GQ1-HT exhibited a fine and uniform martensitic structure, which contrasted sharply with the coarser structures observed after hot-rolling treatment. This transformation suggests that the austenisation process that took place during the reheating step (i.e., 5 min at 880 °C) facilitated the long-distance diffusion of C atoms within the austenite, which led to a uniform distribution. During the subsequent quenching step, the supercooled austenite effectively transformed into martensite. The partial substitution of Nb for Mo appeared to have little impact on the matrix phase of GQ0-HT and GQ1-HT.

Figure 4 shows the TEM images of the steel samples after heat treatment. Both GQ0-HT and GQ1-HT exhibited fine and uniform martensitic structures with clear lath boundaries. The martensitic laths had widths of 150–450 nm. Many nanoscale carbonitrides were observed along dislocations in the laths. In addition, larger second-phase particles were observed at the junctions of several laths, which helped to pin the interface (Figure 4d,g). Ooi and Fourlaris [28] similarly concluded that second-phase particles would inhibit grain growth. Hong et al. [29] concluded that precipitates along grain boundaries were more effective than precipitates within grains at inhibiting grain growth. Large dislocations were distributed around the martensitic packets and inside the laths, which entangled with each other to form dislocation cells (Figure 4b,e,h,k). The strength was further increased by the presence of high-density dislocations on the martensitic laths.

The grain boundaries and lath interfaces of GQ0-HT had coarse carbides with square and spherical shapes ranging in size from 60 nm to 150 nm. Figures 5 and 6 provide elemental mapping analyses of the carbides in GQ0-HT and GQ1-HT, respectively. The carbides in GQ0-HT primarily comprised (Ti, Mo)C, and those in GQ1-HT comprised (Ti, Nb)C. Many studies [17–19] have found that adding Mo in combination with Nb, V and Ti usually results in Mo precipitating as a composite rather than separately in austenite. In GQ1-HT, Mo was not found in the larger precipitates but was mainly distributed in the smaller precipitates.

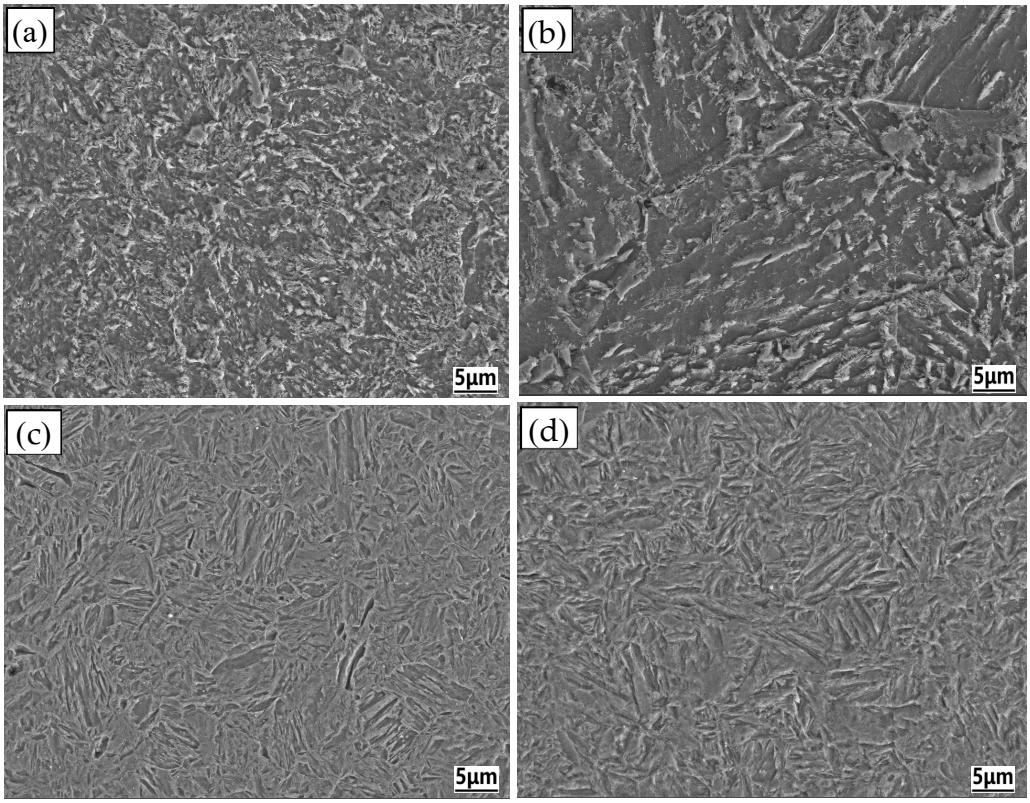

Figure 3. SEM images showing the microstructures of the steel samples: (**a**) GQ0, (**b**) GQ1, (**c**) GQ0-HT and (**d**) GQ1-HT.

Figure 7 shows the inverse pole figure (IPF) maps of the steel samples after hot-rolling treatment and heat treatment. High-angle grain boundaries with orientation differences greater than 15° are indicated by black lines. After hot-rolling treatment, GQ1 had a higher average EGS than GQ0. It is worth noting that GQ0 does not show a uniform microstructure. In contrast, GQ1 exhibits a uniform microstructure, although it has a coarser grain size. After heat treatment, GQ0-HT and GQ1-HT had similar average EGSs that were noticeably smaller than the EGSs after hot-rolling treatment. This observation is corroborated by the grain size distribution graphed in Figure 8, which indicates that the average EGS values of GQ0 and GQ1 were approximately 2.54 and 6.26 μm, respectively. These results indicate that the (Ti, Nb)C particles in GQ1 did not fully exert their pinning effect during the hot-rolling treatment, which resulted in coarser grains. In contrast, the carbide particles in GQ0 were more effective at pinning the grain boundaries, owing to the higher Mo content. At high temperatures, Mo suppresses the disappearance of dislocations, which increases the dislocation density and increases the nucleation positions of Nb(C, N). However, Mo segregation at the interface between Nb(C, N) and ferrite prevents the diffusion of Nb atoms from the ferrite matrix to Nb(C, N), which reduces the activity coefficients of C and N and inhibits the precipitation of Nb(C, N). Thus, GQ0 had smaller and more dispersed precipitates [30,31]. After high-temperature deformation, steel stores deformation energy in the deformation matrix. Deformation energy storage is the driving force for austenite recrystallisation, but it also provides a driving force for deformation-induced precipitation. Thus, there is a competitive relationship between the two processes [32]. When a sufficient hot-rolling temperature is incorporated, the per-pass deformation is sufficient, and per-passes during hot-rolling have been optimised, the suppression of carbon nitride precipitation by Mo enables recrystallisation to store more deformation energy, which results in more complete recrystallisation and better grain refinement. This explains why GQ0 had a smaller average EGS.

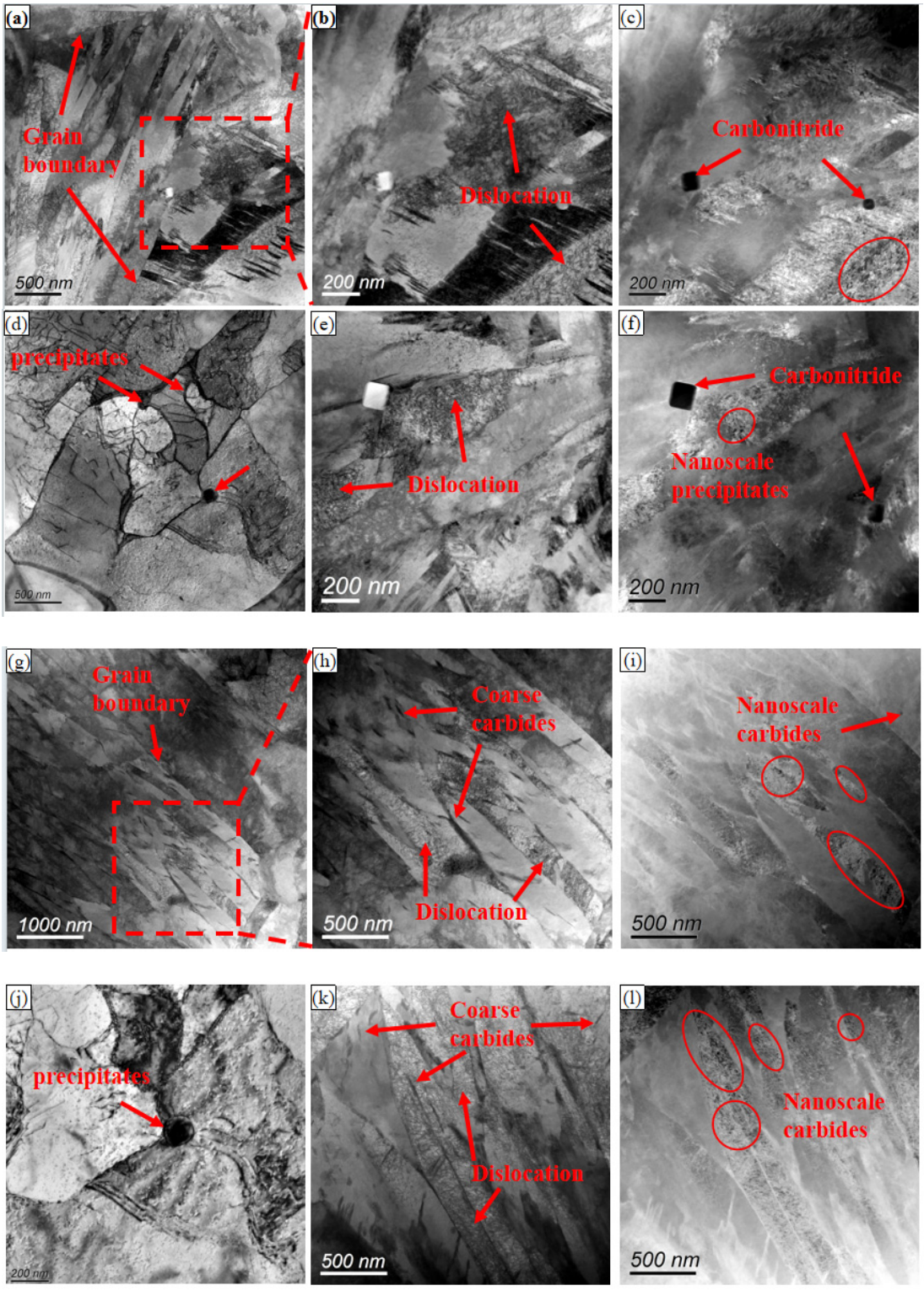

Figure 4. TEM images showing the microstructures of the steel samples after heat treatment: (**a**–**f**) GQ0-HT and (**g**–**l**) GQ1-HT. The first column shows bright-field images, the second column displays local magnifications of the first column and the third column exhibits the corresponding high-angle annular dark-field (HAADF) images of the first column.

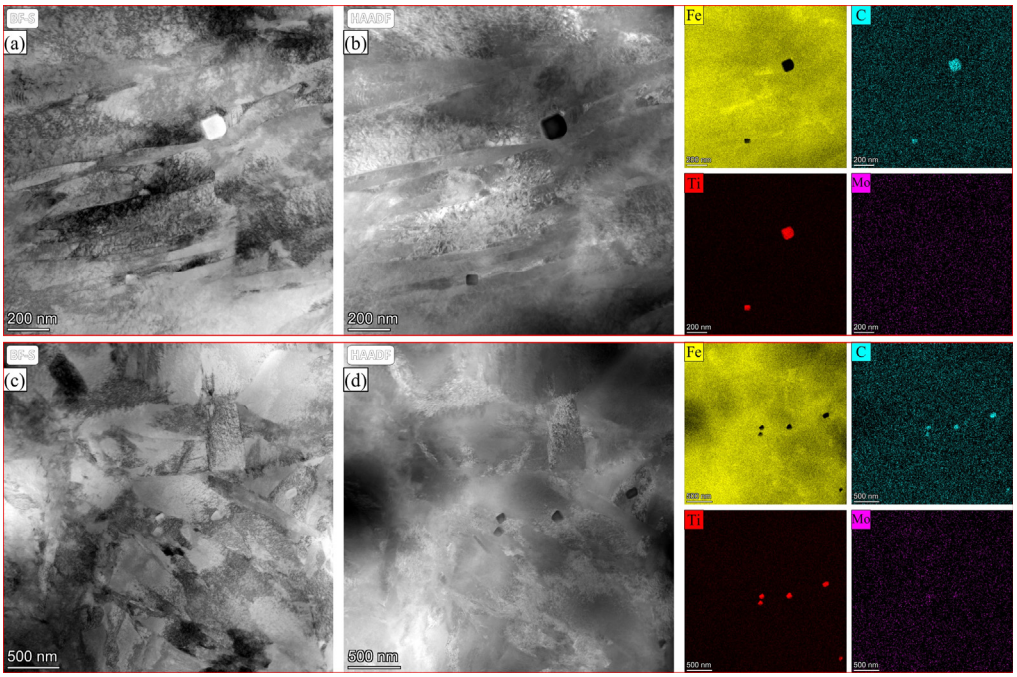

Figure 5. TEM images showing the precipitates of GQ0-HT: (**a**,**c**) bright-field images and (**b**,**d**) HAADF images.

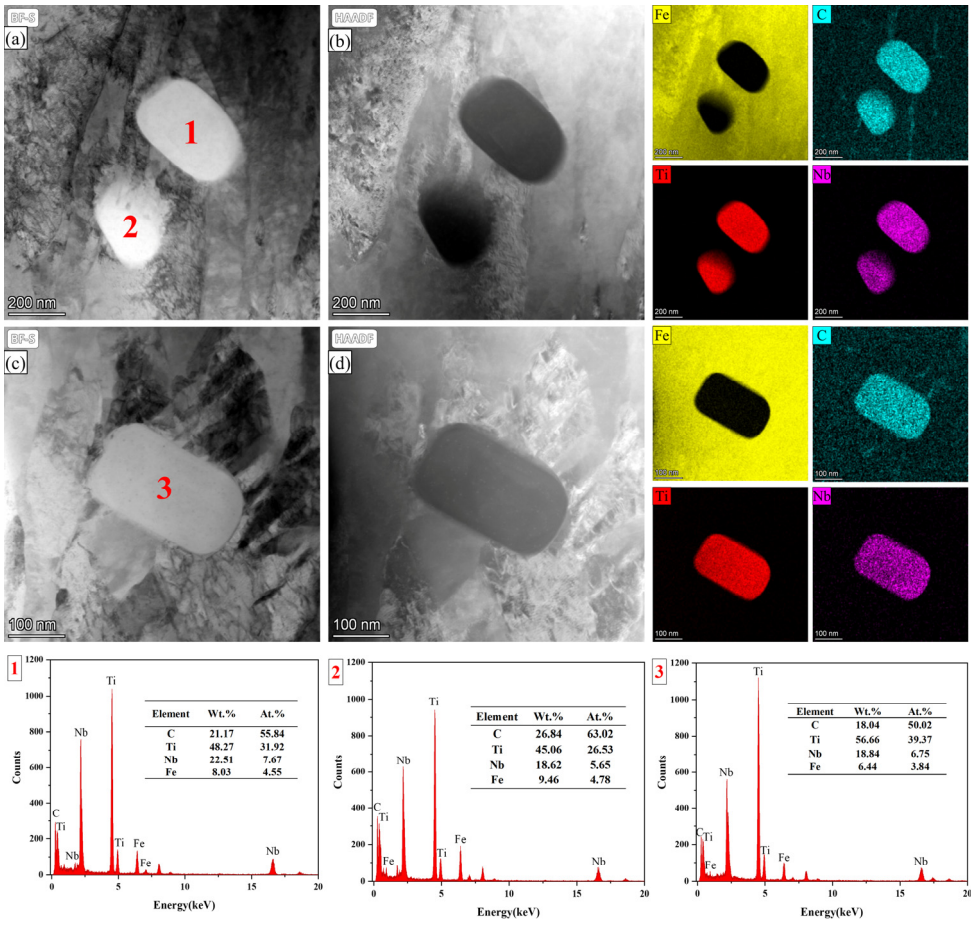

Figure 6. TEM images showing the precipitates of GQ1-HT: (**a**,**c**) bright-field images and (**b**,**d**) HAADF images.

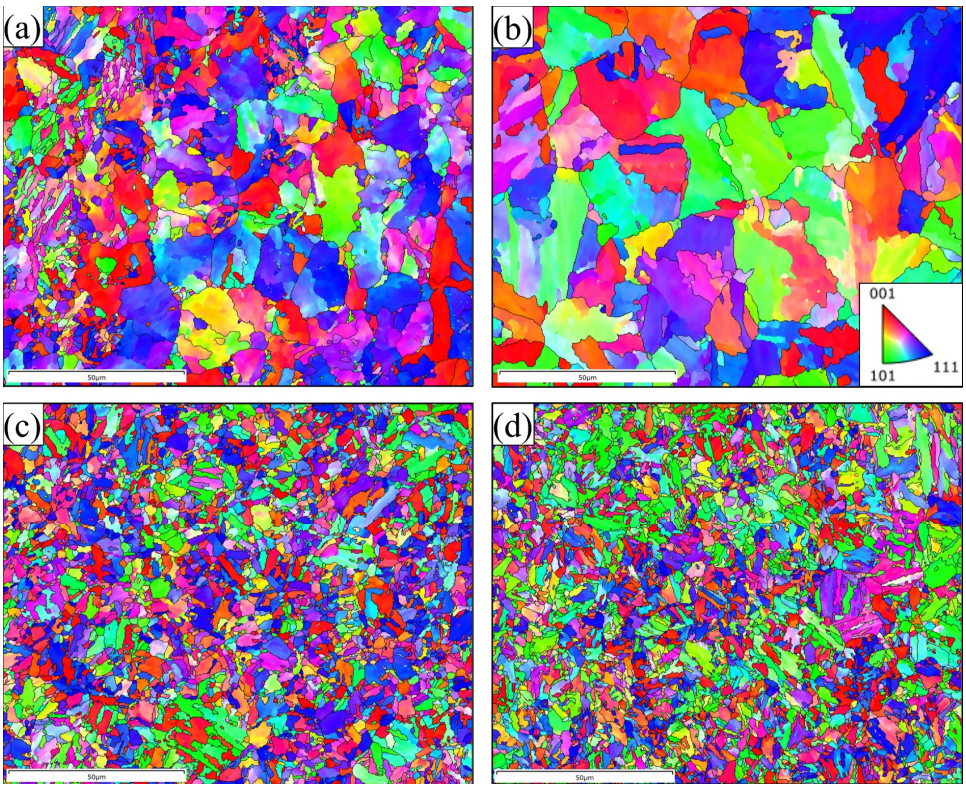

Figure 7. Inverse pole figure (IPF) maps of the steel samples: (**a**) GQ0, (**b**) GQ1, (**c**) GQ0-HT and (**d**) GQ1-HT.

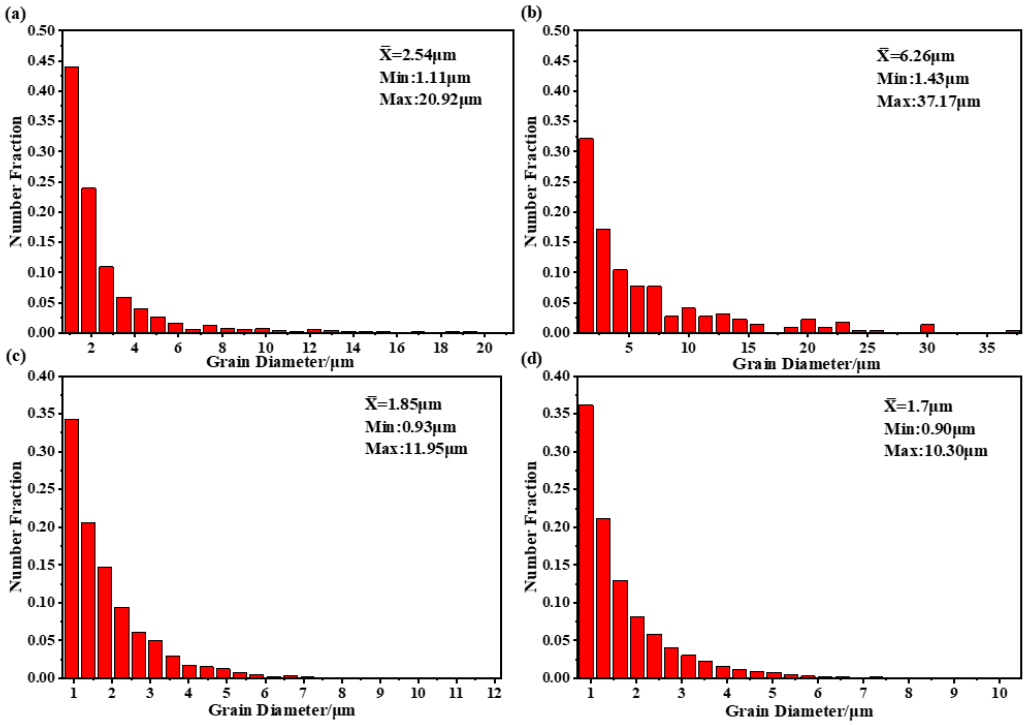

Figure 8. Effective grain size distributions of the steel samples: (**a**) GQ0, (**b**) GQ1, (**c**) GQ0-HT and (**d**) GQ1-HT.

The average EGSs of GQ0-HT and GQ1-HT were 1.85 and 1.7 μm, respectively. The heat treatment transformed the microstructures of GQ0-HT and GQ1-HT into fine and uniform martensite laths, which improved the strength, ductility and toughness of the steels.

Figure 9 shows the EBSD grain boundary distribution maps for two steels. These images clearly depict the distribution of low-angle grain boundaries and high-angle grain boundaries. A comparison reveals a significant increase in the percentage of high-angle grain boundaries after pre-tempering and reheat quenching, indicating a finer substructure within the martensite. A higher percentage of high-angle grain boundaries suggests smaller martensite lath sizes within the substructure [33,34].

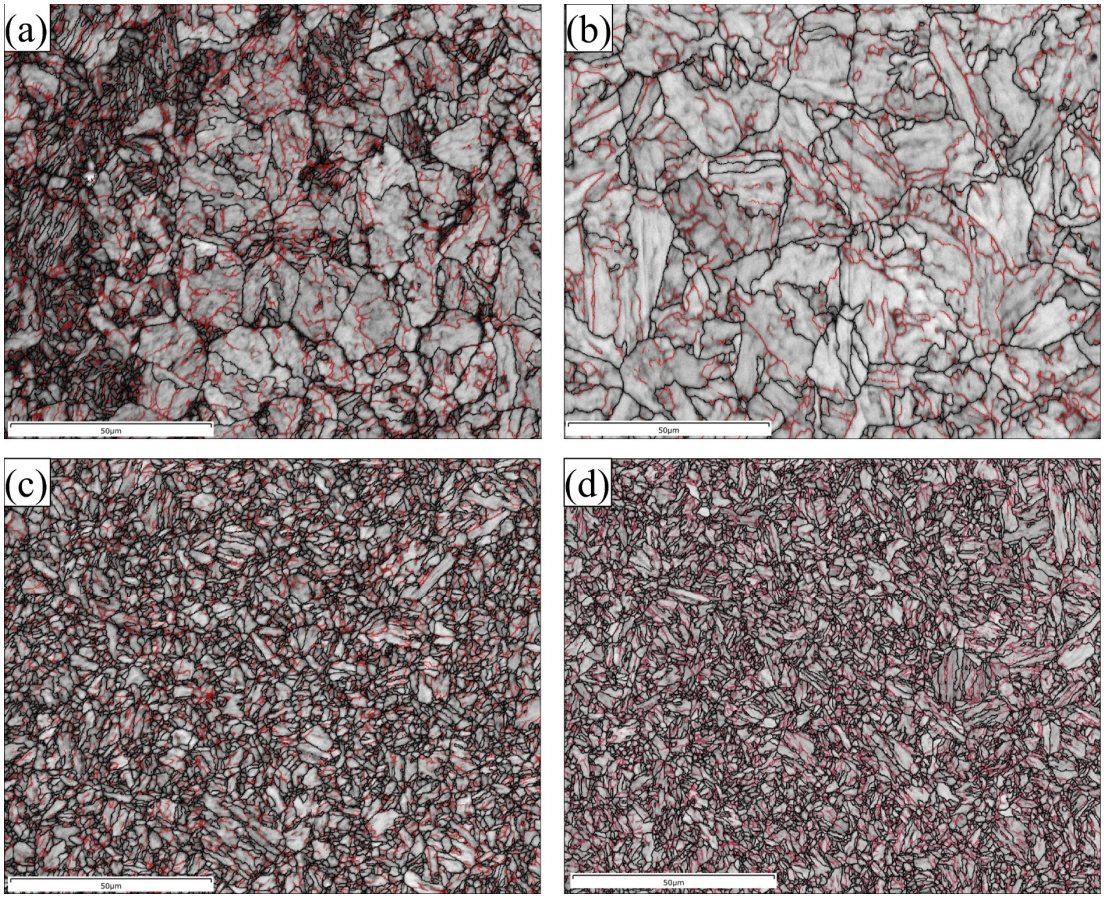

Figure 9. EBSD grain boundary maps of the steel samples: (**a**) GQ0, (**b**) GQ1, (**c**) GQ0-HT and (**d**) GQ1-HT (red lines indicate neighbouring grain orientation differences of 2° to 15°; black lines indicate orientation differences greater than 15°).

Figure 10 presents the distributions of grain boundary misorientations for the steel samples. GQ0 and GQ1 had 60.7% and 50.4% high-angle boundaries, respectively, while GQ0-HT and GQ1-HT had 74.3% and 70.5% high-angle boundaries, respectively. GQ0-HT and GQ1-HT had almost identical distributions of grain boundary misorientations: misorientations of 20°–47° were rare (<2%) while misorientations of 47°–60° were common. In particular, misorientations of 60° reached 11.3% of all grain boundaries. This is characteristic of the martensitic transformation, where the new phase and parent phase maintain the Kurdjumov–Sachs relationship [35]. These results demonstrate that the partial replacement of Mo by Nb can be combined with heat treatment to effectively control the microstructure of the HSLA steel and optimise its properties.

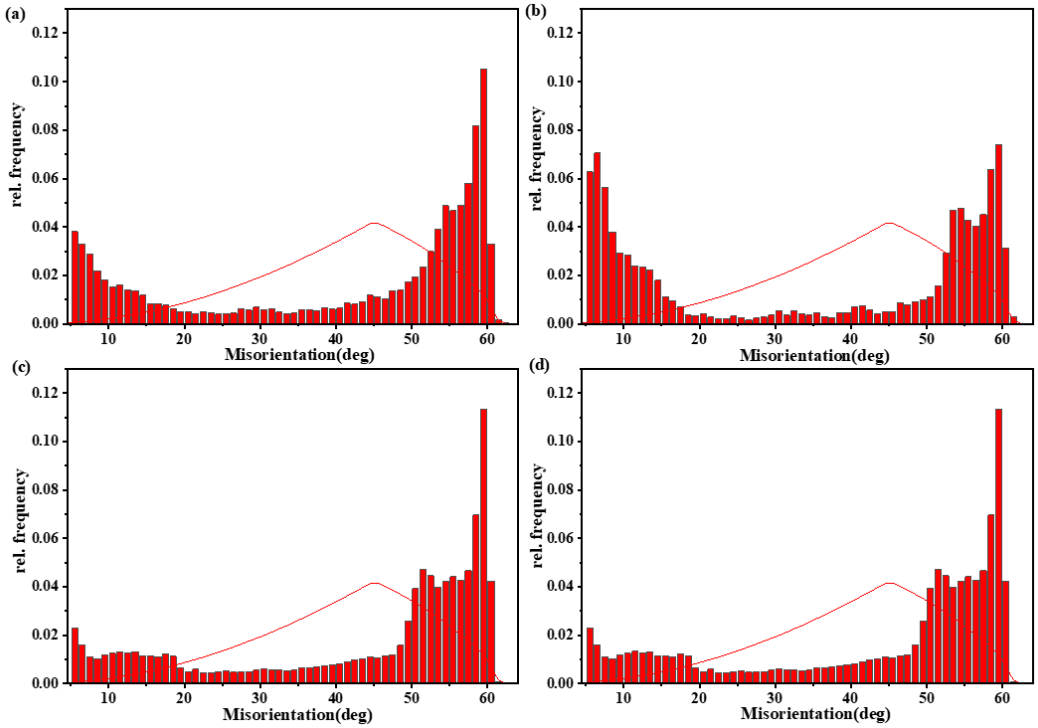

Figure 10. Distributions of grain boundary misorientations for the steel samples: (**a**) GQ0, (**b**) GQ1, (**c**) GQ0-HT and (**d**) GQ1-HT.

3.3. Strengthening and Toughening Mechanisms

Common strengthening mechanisms in high-strength steels include solid-solution strengthening, dislocation strengthening, the precipitation hardening of second-phase particles and grain refinement [35–37]. These strengthening mechanisms can be expressed as follows [38]:

$$\sigma = \sigma_0 + \sigma_s + \sigma_P + \sigma_d + k_y d^{-\frac{1}{2}} \quad (1)$$

where σ is the yield strength of the steel, σ_0 is the internal friction stress of pure Fe, σ_s is the contribution of solid-solution strengthening, σ_p is the contribution from second-phase precipitation hardening and σ_d is the contribution from dislocation strengthening. The final term accounts for grain refinement enhancement where k_y is the Hall–Petch slope and d is the average EGS.

Grain refinement is the crucial mechanism for enhancing the mechanical properties of GQ0-HT and GQ1-HT. According to the Hall–Petch relationship, the relationship between the yield strength (σ_y) and grain size (d) can be expressed as follows [39,40]:

$$\sigma_y = \sigma_0 + \frac{k}{\sqrt{d}} \quad (2)$$

where σ_0 is the base yield strength of a material and k is the Hall–Petch constant related to material hardening. This relationship allows the improvement in yield strength due to grain refinement to be predicted. In this study, the average EGSs of GQ0-HT and GQ1-HT were 1.85 and 1.7 μm, respectively, compared to 2.54 μm for GQ0 and 6.26 μm for GQ1, which indicates substantial grain refinement. GQ1-HT showed a substantial increase in yield strength over GQ1, owing to the greater degree of grain refinement.

The refinements of grains and effective control units can enhance toughness while improving strength. A larger grain size increases the amount of dislocations accumulated in a grain, which increases the stress concentration at the end of the accumulation and in turn increases the probability of cleavage fracture [41]. In contrast, grain refinement

increases the density of grain boundaries, which creates more obstacles that a crack must overcome during propagation and thus enhances the fracture toughness.

Grain boundaries serve as both sources and barriers for dislocations by promoting their accumulation and movement, which manifest as plastic deformation of the material at the macroscopic level. Therefore, grain refinement typically results in better ductility and toughness while achieving high strength. Fine lath bundles not only enhance the strength of martensite but also provide good ductility and toughness. The EBSD results showed that GQ0-HT and GQ1-HT retained 0.36% and 0.33% austenite, respectively, compared to GQ0 and GQ1 retaining 0.28% and 0.18%, respectively. The increase in retained austenite content improved the plasticity of the steel samples to some extent, ensuring that they retained good ductility while possessing ultrahigh strength [42–44].

Carbides play a crucial role in high-strength steels by greatly enhancing the yield strength and hardness [45]. In this study, the second-phase particles contributed not only to precipitation strengthening, but also grain refinement. In the heat treatment, the hot-rolled steel was first tempered to precipitate more second-phase particles in the matrix. The reheating and quenching steps then helped the second-phase particles to pin grain boundaries during the reverse austenisation process and grain growth, which helped to refine the grains and martensite substructure. Table 2 and Figure 11 present the content and size distribution of precipitates obtained by chemical calibration and SAXS.

Table 2. Mass fractions of individual elements in the precipitates of the steel samples (%).

Sample	GQ0	GQ0-HT	GQ1	GQ1-HT
Ti	0.096	0.192	0.088	0.196
Mo	0.112	0.256	0.069	0.144
Nb	-	-	0.034	0.086
C	0.036	0.051	0.039	0.068
N	0.003	0.006	0.004	0.008
Σ	0.247	0.505	0.234	0.502

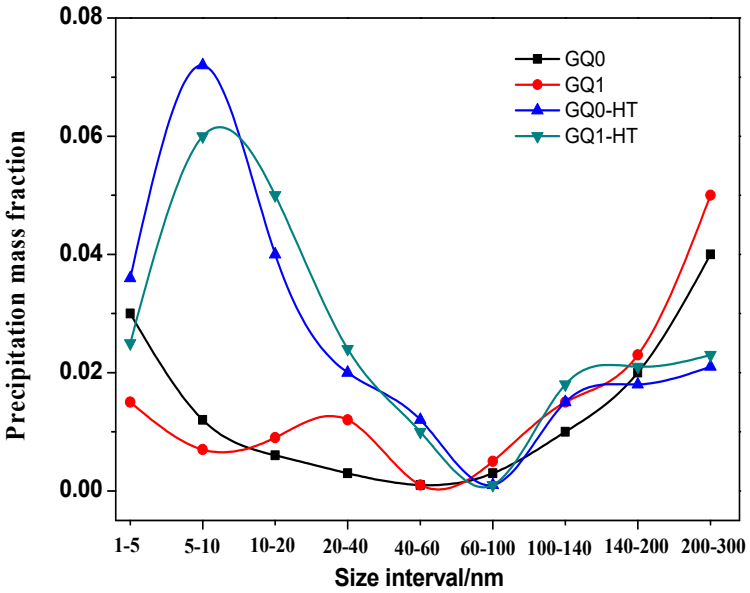

Figure 11. Precipitate size distributions of the steel samples.

The precipitates in GQ0 and GQ1 had relatively low mass fractions of 0.244% and 0.23%, respectively. They mainly precipitated in austenite during the hot-rolling process. Heat treatment greatly increased the mass fractions of the precipitates, which can be attributed to the precipitation of second-phase particles in ferrite or martensite during the tempering process. After tempering, the reverse austenisation further increased the

mass fractions of the precipitates to 0.499% and 0.494%, respectively. Therefore, the heat treatment greatly increased the mass fractions of precipitates in the steel samples.

Figure 11 shows the precipitate size distributions of the steel samples. In GQ0, the precipitates mainly had sizes of 1–10 nm and 140–300 nm, which indicated that fine precipitates were obtained during the hot-rolling process. The precipitates at 140–300 nm were mainly insoluble carbon nitride particles, and they may have included precipitates that grew rapidly in high-temperature austenite. In GQ1, the precipitates mainly had sizes of 1–10, 20–40 and 140–300 nm. GQ0 had more precipitates at 1–20 nm than GQ1, which further confirmed that Mo helped to refine the second phase. In GQ0-HT and GQ1-HT, most precipitates had sizes of 5–40 nm, and especially of 5–20 nm. The heat-treated steel samples had relatively similar precipitate size distributions, which explains why they exhibited similar grain refinement effects.

The austenitic grain size controlled by the second phase can be estimated as follows [46]:

$$D_C = \frac{\pi}{6}\frac{d}{f}\left(\frac{3}{2} - \frac{2}{Z}\right) \quad (3)$$

where D_c is the austenitic grain size, d is the mean diameter of the second phase, f is its volume fraction and Z is a constant whose empirical values are between 1.4 and 2 [14]. According to Equation (3), the critical grain size that can be effectively pinned without substantial growth is directly proportional to the average size of the second phase and is inversely proportional to the volume fraction of the second phase. To reduce the coarsening of the matrix grains, the second-phase particles require a sufficient volume fraction and small size. Therefore, heat treatment is effective in precipitating finer second-phase particles and pinning grain boundaries. These results indicate that the partial substitution of Nb for Mo can be combined with heat treatment to improve the overall mechanical properties of HSLA steels while reducing costs.

4. Conclusions

This study explored the effects of combining a partial replacement of Mo by Nb with heat treatment on the microstructure and properties of HSLA steel. The following conclusions were obtained:

1. Partially replacing Mo with Nb initially resulted in comprehensively lower mechanical properties of HSLA steel after hot-rolling treatment. However, after pre-tempering and reheating and quenching, the heat treatment greatly increased the strength while retaining ductility and toughness, which helped to mitigate the negative effects of replacing Mo with Nb and achieved a good balance between strength, ductility and toughness.
2. The heat treatment increased the percentage of high-angle grain boundaries and decreased the average EGS of the HSLA steels, which enhanced their strength, ductility and toughness. Thus, the partial replacement of Mo by Nb can be combined with heat treatment to effectively control the microstructure of HSLA steels.
3. Heat treatment greatly increased the mass fraction of precipitates, and the precipitates in GQ1-HT and GQ2-HT had similar size distributions. The second-phase particles in these steels were effective at pinning grain boundaries during austenisation, which led to similar grain refinement effects and mechanical properties.

Author Contributions: Conceptualization, F.C.; Methodology, H.F.; Validation, J.Z. and H.F.; Formal analysis, H.F. and J.Q.; Investigation, L.L., J.Z. and F.C.; Resources, Y.L.; Data curation, F.C.; Writing—original draft, L.L.; Writing—review and editing, J.Q.; Supervision, Y.L.; Funding acquisition, J.Q. and Y.L. All authors have read and agreed to the published version of the manuscript.

Funding: This research is sponsored by the National Natural Science Foundation of China (No. 52201114), Guangxi Science and Technology Plan Project (No. AD21238009), and Doctoral Fund Project, Guangxi University of Science and Technology (19Z28), Guangxi Postdoctoral Special fund project (2022039).

Data Availability Statement: The original contributions presented in the study are included in the article, further inquiries can be directed to the corresponding authors.

Conflicts of Interest: The authors declare no conflict of interest.

References

1. Liu, Y.Y.; Wu, J.L.; Wang, D.N. Research on International Mutual Recognition of Carbon Certification System of Automobile Products. *Adv. Eng. Technol. Res.* **2022**, *1*, 364. [CrossRef]
2. Siskos, P.; De Vita, A.; Capros, P. The role of carbon standards on passenger cars towards the reduction of GHG emissions in EU: A model-based scenario analysis. In Proceedings of the 2014 IEEE International Electric Vehicle Conference, Florence, Italy, 17–19 December 2014; pp. 1–8.
3. Lim, S.; Misawa, R.; Furuta, K.; Maruyama, S.; Izui, K.; Nishiwaki, S. Weight reduction design of multi-material vehicle components using level set-based topology optimization. *Struct. Multidiscip. Optim.* **2022**, *65*, 100. [CrossRef]
4. Yildiz, A.R.; Kaya, N.; Öztürk, F. Optimal Structural Design of Vehicle Components Using Topology Design and Optimization. *Mater. Test.* **2008**, *50*, 224–228. [CrossRef]
5. Robinson, A.L.; Taub, A.I.; Keoleian, G.A. Fuel efficiency drives the auto industry to reduce vehicle weight. *MRS Bull.* **2019**, *44*, 920–923. [CrossRef]
6. Viswanadhapalli, B.; Bupesh Raja, V.K. Application of Magnesium Alloys in Automotive Industry-A Review. *Emerg. Trends Comput. Exp. Technol.* **2020**, *35*, 519–531.
7. Vina, V.P.; Nikolaeva, V.B. Effect of heat-treatment conditions on the microstructure and ductility characteristics of steel 45. *Met. Sci. Heat Treat.* **1994**, *36*, 74–78. [CrossRef]
8. Gao, C.; Chen, X.; Chen, X.; Su, C. Microstructure and mechanical properties of as-deposited and heat-treated additive manufactured 9Cr steel. *Mater. Sci. Technol.* **2019**, *35*, 2234–2242. [CrossRef]
9. Sohrabi, M.J.; Naghizadeh, M.; Mirzadeh, H. Deformation-induced martensite in austenitic stainless steels: A review. *Arch. Civ. Mech. Eng.* **2020**, *20*, 124. [CrossRef]
10. Mandal, P.K.; Kant, R. Effect of Microalloying Elements on Mechanical Properties in the High Strength Low Alloy Steel. *Mater. Sci. Forum* **2015**, *830–831*, 231–233. [CrossRef]
11. Wang, S.Z.; Gao, Z.J.; Wu, G.L.; Mao, X.P. Titanium microalloying of steel: A review of its effects on processing, microstructure and mechanical properties. *Int. J. Miner. Metall. Mater.* **2022**, *29*, 645–661. [CrossRef]
12. Sun, L.Y.; Liu, X.; Xu, X.; Li, H.G.; Zhai, Q.J. Review on niobium application in microalloyed steel. *J. Iron Steel Res. Int.* **2022**, *29*, 1513–1525. [CrossRef]
13. Marynowski, P.; Hojny, M.; Dębiński, T. The Effect of Microalloying (Nb, V) and Interstitial (C, N) Elements on Mechanical Properties of Microalloyed Steels. *Arch. Foundry Eng.* **2023**, *23*, 127–136. [CrossRef]
14. Matsuo, S.; Ando, T.; Grant, N.J. Grain refinement and stabilization in spray formed AIS1 1020 steel. *Mater. Sci. Eng. A* **2000**, *288*, 34–41. [CrossRef]
15. Lazarova, R.; Petroy, R.H.; Gaydarova, V. Microstructure and mechanical properties of P265GH cast steel after modification with TiCN particles. *Mater. Des.* **2011**, *32*, 2734–2741. [CrossRef]
16. Rasouli, D.; Khameneh, A.S.; Akbarzadeh, A. Optimization of mechanical properties of a micro alloyed steel. *Mater. Des.* **2009**, *30*, 2167–2172. [CrossRef]
17. Lnoue, K.; Ishikawa, N. Calculation of Phase Equilibria between Austenite and (Nb, Ti, V)(C, N) in Microallyed Steel. *ISIJ* **2001**, *141*, 175–182.
18. Yuan, S.G.; Liang, G.L.; Zhang, X.J. Interaction between elements Nb and Mo during precipitation in microalloyed austenite. *J. Lron Steel Res. Int.* **2010**, *17*, 60–63. [CrossRef]
19. Yoshimasa, F.; Kazuhiro, S. Coarsening behavior of nanometer-sized carbides in hot-rolled high strength sheet steel. *Mater. Sci. Forum* **2007**, *539–543*, 4813–4818.
20. Jung, J.-G.; Park, J.-S.; Kim, J.; Lee, Y.-K. Carbide precipitation kinetics inaustenite of a Nb-Ti-V microalloyed steel. *Mater. Sci. Eng. A* **2011**, *528*, 5529–5535. [CrossRef]
21. Chen, C.Y.; Yen, H.W.; Kao, F.H. Precipitation hardening of high-strengthlow-alloy steels by nanometer-sized carbides. *Mater. Sci. Eng. A* **2009**, *499*, 162–166. [CrossRef]
22. Shi, F.; Zheng, J.; Zhang, J.; Zhao, Y.; Chen, L.Q. Heat Treatment Process, Microstructure, and Mechanical Properties of Spring Steel with Ultra-High Strength and Toughness. *Metals* **2024**, *14*, 180. [CrossRef]
23. Wilzer, J.; Lüdtke, F.; Weber, S.; Theisen, W. The influence of heat treatment and resulting microstructures on the thermophysical properties of martensitic steels. *J. Mater. Sci.* **2013**, *48*, 8483–8492. [CrossRef]
24. Wang, Z.H.; Wang, Y.; Wang, C.M. Grain Size Effect on the Hot Ductility of High-Nitrogen Austenitic Stainless Steel in the Presence of Precipitates. *Materials* **2018**, *11*, 1026. [CrossRef]
25. Matjeke, V.J.; Mukwevho, G.; Maleka, A.; Merwe, J.V.D. Effect of heat treatment on strength and ductility of 52CrMoV4 spring steel. *IOP Conf. Ser. Mater. Sci. Eng.* **2018**, *430*, 012044. [CrossRef]
26. Wang, H.S.; Hsieh, P.J. Establishment of Heat Treatment Process for Modified 440A Martensitic Stainless Steel Using Differential Scanning Calorimetry and Thermo-Calc Calculation. *Metals* **2016**, *6*, 4. [CrossRef]

27. Han, Y.; Shi, J.; Xu, L.; Cao, W.Q.; Dong, H. Effects of Ti addition and reheatingquenching on grain refinement and mechanical properties in low carbon mediummanganese martensitic steel. *Mater. Des.* **2011**, *34*, 427–434. [CrossRef]
28. Ooi, S.W.; Fourlaris, G.A. Comparative study of precipitation effects in Ti only and Ti-V ultra low carbon strip steels. *Mater. Charact.* **2006**, *56*, 214–226. [CrossRef]
29. Hong, S.G.; Jun, H.J.; Kang, K.B.; Park, C.G. Evolution of precipitates in the Nb-Ti-V microalloyed HSLA steels during reheating. *Scr. Mater.* **2003**, *48*, 1201–1206. [CrossRef]
30. Kim, S.; Im, Y.; Lee, S.; Lee, H.; Oh, Y.J.; Hong, J.H. Effects of alloying elements on mechanical and fracture properties of base metals and simulated heat-affected zones of SA 508 steels. *Metall. Mater. Trans. A* **2001**, *32*, 903–911. [CrossRef]
31. Bouyne, E.; Flower, H.M.; Lindley, T.C. Use of EBSD technique to examine microstructure and cracking in a bainitic steel. *Scr. Mater.* **1998**, *39*, 295–300. [CrossRef]
32. Zener, C. Phases and Interfaces: An Interpretation of Microstructure. *Trans. AIME* **1948**, *175*, 47–53.
33. Furuhara, T.; Takayama, N.; Miyamoto, G. Key Factors in Grain Refinement of Martensite and Bainite. *Mater. Sci. Forum* **2010**, *638–642*, 3044–3049. [CrossRef]
34. Pastukhov, V.I.; Khvostov, S.S.; Lobanov, M.L. Effect of Grain Boundaries Type on Carbides Precipitates in Tempered Martensite. *Mater. Sci. Forum* **2019**, *946*, 368–373. [CrossRef]
35. Balasubramanian, N.; Langdon, T.G. The Strength–Grain Size Relationship in Ultrafine-Grained Metals. *Metall. Mater. Trans. A* **2016**, *47*, 5827–5838. [CrossRef]
36. Li, X.C.; Lu, G.Y.; Wang, Q.C.; Zhao, J.X.; Xie, Z.J. The effects of prior austenite grain refinement on strength and toughness of high-strength low-alloy steel. *Metals* **2022**, *12*, 28. [CrossRef]
37. Mohamadnejad, S.; Basti, A.; Ansari, R. Analyses of dislocation effects on plastic deformation. *Multiscale Sci. Eng.* **2020**, *2*, 69–89. [CrossRef]
38. Chen, W.J.; Gao, P.F.; Wang, S.; Zhao, X.L.; Zhao, Z.Z. Strengthening mechanisms of Nb and V microalloying high strength hot-stamped steel. *Mater. Sci. Eng. A* **2020**, *797*, 140115. [CrossRef]
39. Hiramitsu, Y.; Homma, T.; Kamado, S. Improvement of the mechanical properties of Mg-Gd-Y-Zn alloy castings by grain refinement. *IOP Conf. Ser. Mater. Sci. Eng.* **2011**, *21*, 012017. [CrossRef]
40. Nasiri, Z.; Ghaemifar, S.; Naghizadeh, M.; Mirzadeh, H. Thermal Mechanisms of Grain Refinement in Steels: A Review. *Met. Mater. Int.* **2021**, *27*, 2078–2094. [CrossRef]
41. Fairchild, D.P.; Howden, D.G.; Clark, W.A.T. The mechanism of brittle fracture in a microalloyed steel: Part I. Inclusion-induced cleavage. *Metall. Mater. Trans. A* **2000**, *31*, 641–652. [CrossRef]
42. Sohn, S.S.; Song, H.; Jo, M.C.; Song, T.; Kim, H.S.; Lee, S. Novel 1.5 GPa-strength with 50%-ductility by transformation-induced plasticity of non-recrystallized austenite in duplex steels. *Sci. Rep.* **2017**, *7*, 1255. [CrossRef] [PubMed]
43. Kozłowska, A.; Grajcar, A.; Janik, A.; Radwański, K.; Krupp, U. Mechanical and thermal stability of retained austenite in plastically deformed bainite-based TRIP-aided medium-Mn steels. *Arch. Civ. Mech. Eng.* **2021**, *21*, 133. [CrossRef]
44. He, T.T.; Hu, F.; Wang, K.; Zhou, W. High-temperature stability of retained austenite and plastic deformation mechanism of ultra-fine bainitic steel isothermally treated below M_s. *J. Iron Steel Res. Int.* **2024**, *31*, 2014–2030. [CrossRef]
45. Shimotomai, M. Heuristic design of advanced martensitic steels that are highly resistant to hydrogen embrittlement by ε-carbide. *Metals* **2021**, *11*, 370. [CrossRef]
46. Gladman, T. On the theory of the effect of precipitate particles on grain growth in metals. *Proc. R. Soc. Lond. Ser. A Math. Phys. Sci.* **1966**, *42*, 298–309.